

# Dose broadening due to target position variability during fractionated breath-held radiation therapy

W. G. O'Dell,<sup>a,b)</sup> M. C. Schell,<sup>b)</sup> D. Reynolds, and P. Okunieff

*Department of Radiation Oncology, University of Rochester School of Medicine and Dentistry, Rochester, New York 14642-8647*

(Received 30 November 2001; accepted for publication 22 April 2002; published 20 June 2002)

Recent advances in Stereotactic Radiosurgery/Conformal Radiotherapy have made it possible to deliver surgically precise radiation therapy to small lesions while preserving the surrounding tissue. However, because of physiologic motion, the application of conformal radiotherapy to extra-cranial tumors is, at present, geared toward slowing the progression of disease rather than obtaining a cure. At the University of Rochester, we are investigating the use of patient breath-holding to reduce respiratory-derived motion in fractional radiotherapy. The primary targeting problem then becomes the small variation in tumor location over repeated breath-holds. This paper describes the effects of residual target position uncertainty on the dose distribution observed by small extra-cranial tumors and their neighboring tissues during fractional radiation treatment using breath holding. We employ two computational methods to study these effects: numerical analysis via Monte Carlo simulation and analytical computation using three-dimensional convolution. These methods are demonstrated on a 2-arc, 10-fraction treatment plan used to treat a representative lung tumor in a human subject. In the same human subject, the variability in position of a representative lung tumor was measured over repeated end-expiration breath-holds using volumetric imaging. For the  $7 \times 7 \times 10$  mm margin used to treat this 12 mm diameter tumor and the measured target position variability, we demonstrated that the entire tumor volume was irradiated to at least 48 Gy—well above the tumoricidal threshold. The advantages, in terms of minimizing the volume of surrounding lung tissue that is radiated to high dose during treatment, of using end-expiration breath holding compared with end-inspiration breath-holding are demonstrated using representative tumor size and position variability parameters. It is hoped that these results will ultimately lead to improved, if not curative, treatment for small (5–20 mm diameter) lung, liver, and other extra-cranial lesions. © 2002 American Association of Physicists in Medicine. [DOI: 10.1118/1.1485977]

**Key words:** 3D conformal radiotherapy, dose distribution analysis, lung cancer, motion-correction, radiation therapy dose calculations

## I. BACKGROUND AND SIGNIFICANCE

Recent advances in Stereotactic Radiosurgery/Conformal Radiotherapy have made it possible to deliver surgically precise radiation therapy to small lesions while preserving function to surrounding structures. This radiosurgical approach is used routinely by physicians to eradicate small, stationary lesions in the cranium. Unfortunately, the application of 3D conformal radiotherapy to isolated tumors in the chest and abdomen is, at present, geared toward slowing the progression of disease rather than obtaining a cure. This is because these organs can experience significant physiologic motion, thwarting the benefits of current approaches to conformal therapy. The primary source of this motion is respiration. In the treatment of lung and liver tumors, the traditional therapeutic approach is to measure the range over which the tumor moves during the respiratory cycle and to then irradiate a volume that encloses the entire tumor over its entire motion range. The oncologist's dilemma is that in prescribing a lethal radiation dose to the tumor, a sufficiently large volume of healthy tissue would be damaged to cause significant clinical repercussions, including organ failure. In our radiation treatment center we are investigating the use of patient

breath holding to reduce respiratory-derived motion during fractionated radiotherapy. The primary targeting problem then becomes the small variation in tumor location from one breath-hold to the next. Previous research had focused on the dose effects from relatively large target position uncertainties resulting from respiration and bladder/bowel motions. These studies involved comparatively large lesions (typically  $\sim 10$  cm diameter) such as primary cancer of the prostate,<sup>1–6</sup> liver,<sup>7,8</sup> lung,<sup>5</sup> nasopharynx,<sup>9</sup> and esophagus.<sup>2</sup> The sizes of the lesions involved precluded the use of lethal doses of radiation, thereby the aims in these earlier studies were to achieve the optimum trade-off between therapeutic response and complication risk. In contrast, our investigations involve smaller, 5–20 mm diameter lesions wherein the intent of treatment is the ablation of the target, with minimization of radiation damage to the surrounding tissue as an important, but secondary concern. In the present study, our aim is to model the effects of target repositioning variability due to breath-hold reproducibility error on the dose field observed by small metastatic lung lesions and surrounding tissue in hopes that this will ultimately lead to an improved under-

standing of this phenomenon and improved approaches to clinical radiotherapy planning of similarly sized lesions.

### A. Cancer statistics

According to American Cancer Society statistics,<sup>10</sup> lung cancer will account for the second greatest number of new cancer cases for both men and women this year (followed only by prostate cancer in men and breast cancer in women). Lung cancer has surpassed breast cancer as the leading cause of cancer death in women and is expected to account for 25% of all female cancer deaths in 2002. It is estimated that 85% of all new lung cancer patients will die from their cancer.<sup>11</sup> The lungs are also the second most frequent site of metastatic disease and, in 20% of these cases, the lungs are the only site of metastases.<sup>12</sup> The liver is the most prevalent site of metastasis, with autopsy series reporting a range of 30% to 70% for all patients who die of cancer.<sup>13</sup> For example, colorectal cancer is among the top four cancers in both incidence and death rates. However, death is usually the result of metastases, and in 80% of these patients (19 200 people per year) the liver is the only site of metastases.<sup>14</sup> Similar data is available for breast cancer wherein 40% of patients with metastases eventually develop liver disease and 80% eventually develop lung disease.<sup>15</sup>

### B. Impact of aggressive therapy

Aggressive management of lung and liver metastases is likely to significantly improve the survival and quality of life for these patient groups.<sup>16</sup> It has been shown that in colorectal cancer patients with isolated metastases to the liver, curative resection of the liver lesions leads to 30–40% 5-year survival<sup>17</sup> and a complete freedom from disease in 30% of these patients.<sup>14</sup> Unfortunately, 75–80% of all liver lesions are deemed unresectable due to their anatomic location and size and/or because of disease-associated hepatic cirrhosis, hyperbilirubinemia, and physical weakness that prevents surgical intervention. Faced with a significant risk of morbidity and mortality, patients often choose to forego surgery. Since there is currently no long-term effective chemotherapy for primary or metastatic liver cancer, there is very little that can be done for patients with unresectable liver tumors. If one takes into account the successes and failures of treatment for metastatic disease over the past 20 years, the technically sophisticated but intellectually simple concept of locally sterilizing metastatic disease using external-beam radiotherapy has the potential of outperforming many, if not all, of the advances in the field of the past two decades.

## II. METHODS

The target position probability density was modeled as a three-dimensional (3D) ellipsoidal Gaussian distribution. The effect of randomized target repositioning was assessed through numerical simulation using Monte Carlo analysis and through analytical computation using 3D convolution. These methods were demonstrated on a representative 2-arc, 10-fraction treatment plan that was used to treat individual tumors in a human subject presenting with multiple meta-

static lung lesions. The effect of the magnitude of the position variability on the changes in the observed dose was studied using standard deviations in tumor position that ranged from 1 to 4 mm. For the same human subject, tumor position variability data was gathered from pretreatment magnetic resonance image (MRI) datasets. The measured variability values were also applied in the analysis. Using representative tumor position variability values and corresponding margin definitions, a comparison was made between the volumes of lung tissue that would be expected to receive harmful doses of radiation using end-expiration breath holding versus end-inspiration breath-holding during treatment planning and radiation delivery. Dose volume histograms (DVHs) were employed to assess exposure to both the target and the surrounding healthy tissue, as well as to compare the results across the various methods.

### A. Target position variability model

For fractionated radiotherapy with breath-holding, the variability in position of the target over all the repeated breath-holds was modeled as a Gaussian distribution. The standard deviation in position about the mean position was allowed to vary independently with coordinate direction, where the coordinates were defined with respect to the patient: Superior–inferior (SI); anterior–posterior (AP); and right–left (RL). The resulting 3D Gaussian ellipsoid was sampled at 1 mm intervals in each direction to create a digitized position probability matrix. It is important to sample the Gaussian probability matrix out a sufficient distance to ensure that the target position probability at the edge voxels is very small. This was achieved by sampling out to a distance equal to 3 times the Gaussian standard deviation. For the 4 mm position variability model, the Gaussian probability matrix was generated over 25×25×25 grid where each voxel corresponds to 1 cubic millimeter.

### B. Dose perturbation via convolution

As the number of treatment fractions approaches infinity, the cumulate dose seen by the target can be modeled as the convolution of the 3D dose distribution with the 3D Gaussian probability distribution for target position, as described previously by several authors.<sup>1,2,5,8</sup> The convolution operator is described by the equation<sup>18</sup>

$$\begin{aligned} \mathbf{f}[l,m,n] &= \mathbf{g}[l,m,n] \otimes \mathbf{h}[i,j,k] \\ &= \sum_i \sum_j \sum_k \mathbf{h}[i,j,k] \cdot \mathbf{g}[l-i,m-j,n-k], \quad (1) \end{aligned}$$

where  $\mathbf{g}$  is the original (planned) dose field represented as a 3D matrix (of size  $L \times M \times N$ ) of dose values,  $\mathbf{h}$  is the 3D Gaussian distribution model represented by a 3D matrix of size  $I \times J \times K$ , and  $\mathbf{f}$  is the resulting, altered dose distribution. The values of  $I$ ,  $J$ , and  $K$  increase (decrease) with increasing (decreasing) position variability in the SI, AP, and RL directions, respectively. The analyses using convolution and the generation of dose field plots and their derivatives were per-

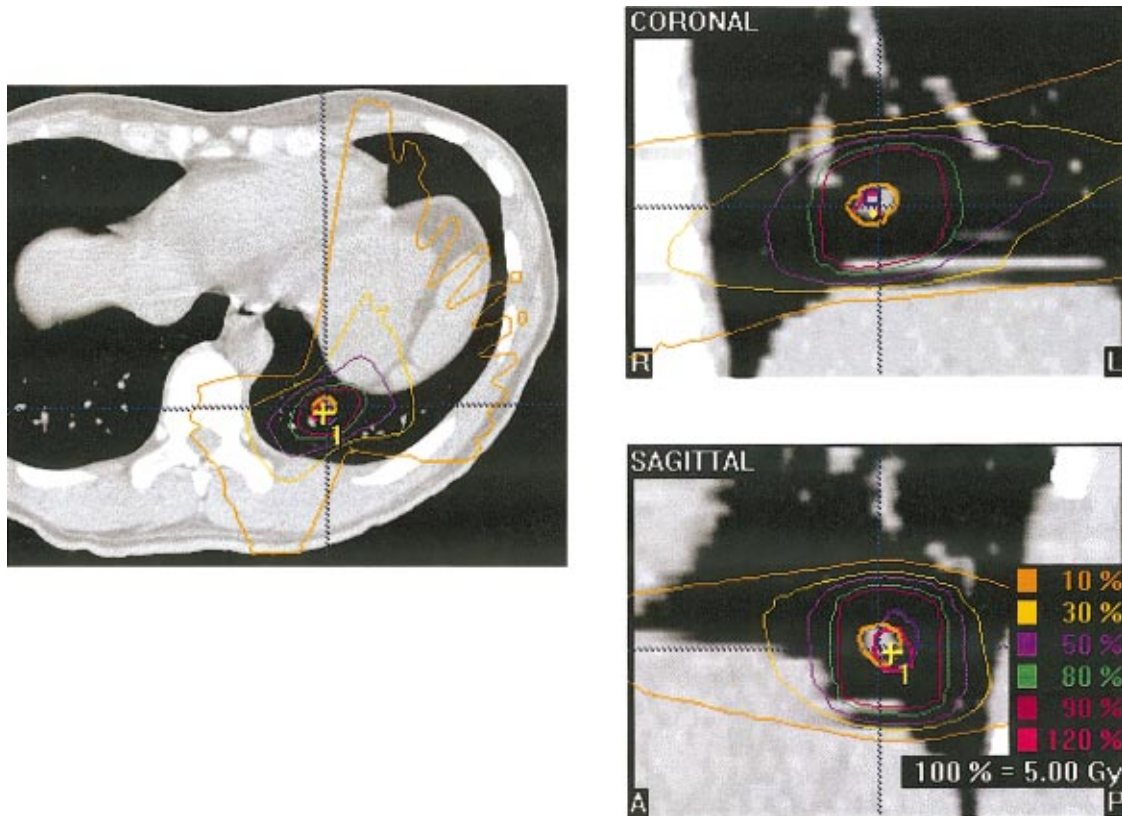


FIG. 1. Isodose contours overlaid onto a CT image of lung of cancer patient. 100% dose=5 Gy. The yellow arrow and central pink contour were manually defined to mark the location of one  $\sim 1$  cm diameter tumor. The central purple and orange contours mark the location of the tumor in subsequent CT image acquisitions. The surrounding contours (red, green, purple, yellow, and orange) are the isodose contours as described in the legend.

formed using dedicated Java code written by the authors and based on the NIH ImageJ software package (developed at the U.S. National Institutes of Health and available on the Internet at <http://rsb.info.nih.gov/ij/>).

### C. Target position variability via Monte Carlo simulation

The dose field perturbation for a finite number of treatment fractions can be assessed using Monte Carlo simulation, as demonstrated by Leong,<sup>19</sup> and others<sup>4,8,9</sup> and validated against the convolution method by Bel,<sup>3</sup> Lujan,<sup>7</sup> and McCarter *et al.*<sup>6</sup> A random-number generator was modified to produce both negative and positive output displacements that fall within a prescribed Gaussian distribution.<sup>20</sup> The generator's output was used to shift the prescribed dose field in each of the SI, AP, and RL directions randomly for 10, 20, 100, or 1000 treatment fractions. The method of Monte Carlo simulation applied to a digitized dose field requires displacements of the target to be integer valued. The numbers returned from the random number generator were first scaled to fit the desired Gaussian distribution and then rounded to the nearest whole number. This analysis was performed using Microsoft Visual Basic running within Excel.

### D. Lung lesion treatment plan

A realistic treatment 3D dose field was obtained from a conventional conformal beam treatment plan for a representative lung lesion in a human subject. The selected lesion was approximately 12 mm in diameter and located posteriorly inferiorly in the patient's left lung. The treatment plan for this lesion consisted of 6-MV X rays applied in two, 110-degree arc pathways separated by 20 degrees. The clinical target volume (CTV) was defined by the observable tumor as manually segmented using the commercial planning system software. The planning target volume was defined as the CTV with a margin specification of  $7 \times 7 \times 10$  mm in the AP, RL, and SI directions, respectively. The plan was created using the BrainLAB Novalis system and BrainScan 5.0 software and implemented at the University of Rochester's R. J. Flavin Novalis Shaped Beam Surgery Center. Each arc was administered daily, during independent 15 second breath-holds. The external beam radiation was administered daily over 10 days of treatment to give a total dose to the lesion of 50 Gy. A diagram of the treatment plan dose distribution is shown in Fig. 1. Patient repositioning between treatment days was performed using BrainLAB's ExacTrac Patient Positioning System (EPPS). The EPPS tracks skin-affixed retro-reflective markers with a pair of infrared cameras. The Nova-

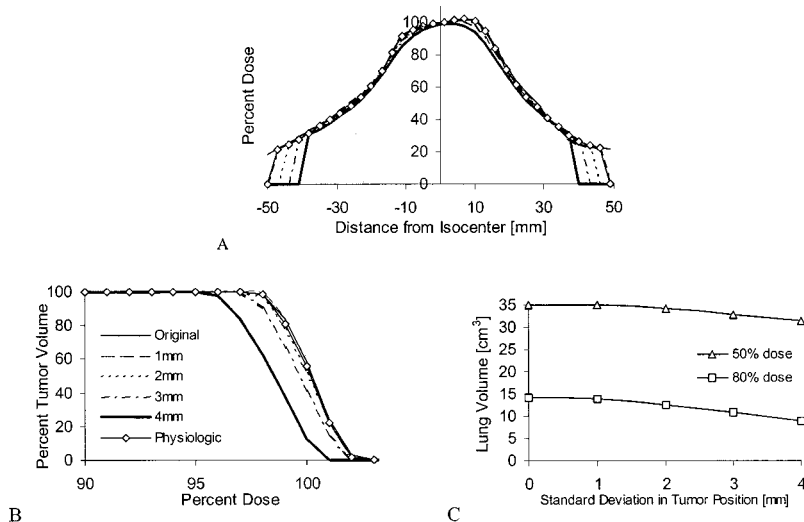


FIG. 2. (A) Dose profiles across the central slice for the planned dose distribution of lung lesion 1 and target position variability of 1–4 mm in each direction (“1, 2, 3, 4 mm”) and for the measured position variability (“Physiologic”). (B) Dose-volume histogram of the tumor for the corresponding studies. (C) Plots of the absolute volume of surrounding lung tissue exposed to 50% and 80% doses, as a function of the amount of tumor position variability.

lis unit was designed for stereotactic radiosurgery with an alignment tolerance of 0.75 mm. The EPPS positioning uncertainty is typically 0.5 to 1.5 mm.

### E. Lung lesion position variability measurements

Prior to radiation therapy, repeated volumetric MRI datasets of the lungs were acquired in the patient volunteer. All procedures were performed in accordance with federal and university guidelines and the patient had given informed consent. The three sets of chest MRI volume data were acquired during  $\sim 30$  second periods of patient breath-hold at relaxed end-expiration. The patient volunteer was instructed to perform two deep breaths followed by a relaxed expiration and breath-hold. Each MRI 3D dataset consisted of 168 overlapping sagittal slices with slice thickness 4 mm and slice center-to-center separation of 1 mm. For each of the five lesions, the centroid was manually demarked and the mean position and standard deviations about the mean position were then computed.

### F. End-expiration breath-holding versus deep end-inspiration breath-holding

A secondary hypothesis is that the improved target localization with end-expiration breath-holding (EEBH) and accompanying reduction in treatment margin will more than compensate for the decreased lung density but larger margins associated with deep end-inspiration breath-holding (DIBH). The current literature provides no quantification of the motion of isolated tumors in the lung and/or liver during respiration, nor of tumor position reproducibility over multiple breath-holds. However, studies have been performed looking at diaphragm position during free breathing and over repeated breath-holds, suggesting that target position variability is improved with EEBH compared to DIBH. Using these values, treatment plans were constructed using conventional margin specifications to ablate the representative lung lesion. Lung density changes from end-expiration to deep inspira-

tion were included in the estimate of the volume of surrounding lung tissue exposed to high dose in each treatment approach.

## III. RESULTS

### A. Target position variability and dose broadening

The result of the convolution of the dose matrix by the position variability matrix is an eroded version of the original dose distribution, as depicted in Fig. 2(A) and as described by previous authors.<sup>1,19</sup> The target position variability alters the original dose distribution by increasing the dose field width at the lower doses, reducing the width at the higher doses, and decreasing the slope of the dose profile edges. Figure 2(A) shows a comparison of the original and eroded profiles for standard deviation in position (ranging from 0–4 mm) computed using the convolution equation. The effect of target position variability on the cumulative dose seen by the target is depicted by the corresponding DVHs for the target. The relationship between the leftward shift of the tumor DVH curve and the magnitude of the position variability is monotonic but nonlinear, as seen quantitatively in Fig. 2(B). The decrease in the dose at the 50% tumor volume at 1 mm target position standard deviation is less than 0.2%, but the decrease in dose becomes 1.7% for a standard deviation of 4 mm. The volume of surrounding tissue receiving  $\geq 50\%$  dose and that receiving  $\geq 80\%$  dose dropped as the position standard deviation increased, as plotted in Fig. 2(C).

### B. Finite versus infinite number of treatment fractions

Figure 3(A) shows a comparison of the original and shifted tumor DVHs for a 4 mm standard deviation in position computed using both the convolution equation and Monte Carlo method using single trials at 10, 20, 100, and 1000 fractions. The results for the 100-fraction and the 1000-fraction Monte Carlo runs were nearly identical, suggesting that 100 fractions are sufficient to achieve convergence for this approach. The DVH values and dose profiles for the

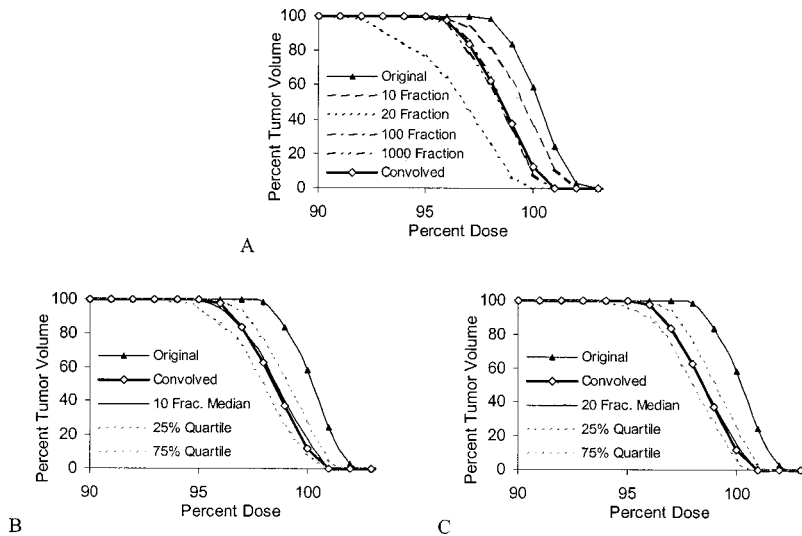


FIG. 3. (A) DVH of the tumor for target position standard deviation of 0 mm ("Original") and 4 mm as computed using the Monte Carlo method with randomly chosen trials of 10, 20, 100, and 1000 fractions, and using convolution. DVH plots including the mean and quartile curves for 50 repeated trials of (B) 10-fraction and (C) 20-fraction Monte Carlo runs. Mean and quartiles were computed with respect to varying percent tumor volume for a fixed dose percentage.

convolution method were indistinguishable from those of the 1000-fraction Monte Carlo method, determining the equivalence of the approaches. There is a statistical relationship between the expected results from any given 10-fraction simulation and the finite-fraction results (the convolution method), as described by sampling theory. Namely, the expected standard deviation of the mean,  $\sigma_M$ , for  $N$  number of fractions is given by  $\sigma_M^2 = \sigma_P^2/N$ , where  $\sigma_P$  is variance of the total population. To better illustrate this phenomenon, 50 trials using 10 fractions were conducted using the Monte Carlo approach. From the 50 trials, the mean, 25th quartile, and 75th quartile DVH curves, computed as percent tumor volume varying as a function of percent dose, were compiled and plotted in Fig. 3(B) along side the DVH curve computed using the convolution method. This analysis was repeated for 50 runs of 20 fractions and the results for these are plotted in Fig. 3(C). These graphs give the expected spread in the DVH outcomes associated with using a finite number (10 or 20) of treatment fractions. The randomly chosen 20-fraction trial shown in Fig. 3(A) happens to lie outside the 20-fraction quartile range shown in Fig. 3(C), but this is not unexpected in light of the sampling theory.

### C. Lung lesion position variability measurement and dose broadening

Breath-holding for the duration of the MRI acquisition ( $\sim 30$  seconds) was well tolerated by the patient volunteer. As shown in Table I, the average variability in position for all five lesions and over three repeated breath-holds was found to be less than 3 mm in any direction, with the greatest

variability in the superior–inferior direction compared to the anterior–posterior and lateral directions. Our findings are comparable to those found by Holland *et al.*<sup>21</sup> and Balter *et al.*<sup>22</sup> for position reproducibility of the diaphragm. Lesion 1, shown in Fig. 1, was a 12 mm diameter tumor with position standard deviations of 2.5, 1.3, and 0.8 mm in the SI, AP, and RL directions, respectively. At physiologic variability values, the percent of tumor volume seeing 100% of the dose (50 Gy) was 44%, compared to 56% for a fixed target. However, in both cases all of the tumor volume observed  $\geq 96\%$  dose (or 48 Gy)—above the tumoricidal threshold.

### D. End-expiration breath-holding versus end-inspiration breath-holding

With breath-holding protocols, the reproducibility of the end-expiration location of the diaphragm from breath-hold to breath-hold is less than 0.4 mm, while that for end-inspiration is approximately 1.3 mm.<sup>22</sup> The diaphragm also moves *during* a breath-hold. During a relaxed breath-hold at end-expiration (EEBH) the diaphragm displaces superiorly at a rate of  $0.15 \text{ mm/s} \pm 0.7 \text{ mm/s}$ .<sup>21</sup> This leads to an overall shift in the superior–inferior direction of  $1.9 \text{ mm} \pm 1.4 \text{ mm}$  for a 20-second breath-hold. For breath-holds at relaxed end-inspiration, the total displacement is  $2.3 \text{ mm} \pm 1.2 \text{ mm}$  with a very nonlinear velocity profile. Korin *et al.* also performed a preliminary study looking at the global motion of the liver. They found that the motion of the liver follows closely that of the diaphragm during relaxed breathing, with SI motion dominant, and AP and RL motions  $< 2 \text{ mm}$ .<sup>23</sup> In comparison, Hanley *et al.*<sup>24</sup> reported that diaphragm repositioning error

TABLE I. MRI-based measurement of reproducibility of lesion position over multiple end-expiration breath-holds. Values are given as standard deviation (in mm) of position about the average position, over 3 trials.

	Lesion 1	Lesion 2	Lesion 3	Lesion 4	Lesion 5
Superior–inferior	2.5	2.9	2.0	2.0	2.2
Anterior–posterior	1.3	2.1	2.8	1.4	1.3
Lateral	0.8	1.5	1.5	0.8	0.8

for repeated deep inspiration breath-holding (DIBH) was 2.5 mm and that motion during each breath-hold was 1.0 mm (standard deviation about the mean position). These DIBH studies were performed using a spirometer to improve the reproduction of inspiration levels. A conservative treatment plan would entail specifying a planning target volume (PTV) with treatment margins around the tumor equal to two times the expected standard deviation in position plus two times the expected motion range. First, using a back-of-the-envelope comparison of planning target volumes, we consider a 12 mm diameter clinical target volume. Using the inspiration data from Balter's and Holland's papers (1.3 mm and 2.3 mm, respectively), 7.2 mm of margin would be needed. This leads to a planning target volume of 9.6 cm<sup>3</sup>. The corresponding margin for an end-expiration breath-hold, based on Balter's and Holland's results (0.4 mm and 1.9 mm, respectively), would be 4.6 mm, giving a planning target volume of 5.0 cm<sup>3</sup>. This represents a reduction in healthy tissue volume within the PTV of 4.6 cm<sup>3</sup>, or 53%, using the EEBH plan compared to the DIBH plan. For an expected decrease in DIBH lung density of 26% (Ref. 24) compared with the EEBH technique, the DIBH technique would result in a less favorable lung mass exposure compared with the end-expiration breath-holding approach. For a 20 mm diameter CTV (perhaps more reasonable for this 12 mm lesion considering the inherent inaccuracies in the diagnostic imaging system and the potential for microscopic extent of the disease) the same analysis gives a reduction in healthy tissue volume being irradiated of 8.3 cm<sup>3</sup>, or 48%, when using EEBH compared to DIBH. With the inclusion of dose spread effects, the results were similar. Two treatment plans were created for the representative lung lesion in the manner described earlier but with axisymmetric treatment margins of 4.6 and 7.2 mm, to represent the EEBH and DIBH plans, respectively. The treatment plan with the 4.6 mm margin was then convolved with a Gaussian target position variability model with an axisymmetric target position standard deviation of 2.3 mm. This was repeated for the 7.2 mm margins plan and a 3.6 mm standard deviation of target position. For the EEBH case the absolute volume of surrounding lung tissue receiving  $\geq 50\%$  dose was 9.4 cm<sup>3</sup>. That for the DIBH values, after adjustment for the 26% decrease in lung tissue density due to increase air volume, was 12.4 cm<sup>3</sup> (a difference of 24%). For the volume of lung tissue receiving  $\geq 80\%$  dose, the EEBH and DIBH methods gave 2.39 and 3.15 cm<sup>3</sup>, respectively: a difference again of 24% and very similar to the back-of-the-envelope calculation result above.

## IV. DISCUSSION

### A. Preliminary clinical results

The clinical radiotherapy plan and short-term outcome for the initial patient subject have been presented in detail previously.<sup>25</sup> In regards to the measurement, modeling, and

verification of the dose broadening effect, the results were as follows. A treatment margin specification of  $7 \times 7 \times 10$  mm, in the AP, RI, and SI directions, respectively, was chosen by the attending physicians. The target repositioning variability results from the repeat end-expiration MRI datasets indicate that these margins represent a size equal to or greater than three times the expected standard deviation in position. For a typical 12 mm diameter tumor, this size margin would ensure that the entire tumor remains within the high-dose region for each fraction with 99.87% certainty, assuming that sources of target position variability other than that due to breath-holding error are negligible. The results presented in this paper demonstrated that the entire tumor volume was irradiated to a minimum of 48 Gy—well above the tumoricidal threshold. This finding was substantiated by the clinical results: there was evidence of tumor shrinkage during treatment and all but one of the lesions had disappeared completely by the end of the 10-day therapy. At the 6-month and 12-month follow-ups, all five lesions had been eradicated with no indication of disease recurrence at the treatment sites.

### B. Edge effects

As described in detail by Lujan *et al.*,<sup>7</sup> artifacts will occur at the boundaries of the dose field when the dose does not fall to zero smoothly, such as occurs at the surface–air interface and at the edges of the sampled dose field. The size of the boundary zone where artifacts may appear is determined by the standard deviation ( $\sigma$ ) of the target position probability distribution and for most practical purposes is limited to  $3\sigma$ . In the current study, the dose field was sampled over a  $10 \times 10 \times 10$  cm region centered about the lung lesion. For simplicity of the calculation using the convolution and Monte Carlo methods, the dose values for locations outside the sampled dose field were assumed to be zero. However, the measured dose on the perimeter of the sampled dose field was found to be significant at some locations, with a maximum dose at the border of the sampled region of 41%. The error is reflected in Fig. 2(A) where there is an abrupt dose profile drop-off at the outer-most 2–7 mm of the measured dose profiles. This solution to the edge artifact is to sample the dose field out into the zero-valued regions, or at least sufficiently far from the target and the lung volumes so that the edge effects do not corrupt the DVH results. The limited spatial extent of the dose field sampling also prevents an accurate determination of the lung tissue DVH values for doses less than  $\sim 41\%$ , although the spatial extent of the sampling was sufficient for an accurate determination of all tumor DVH values and lung tissue DVH values  $\geq 50\%$ . In addition, because of the relatively small size of the planning target volume compared with the entire left lung volume, 12 cm<sup>3</sup> versus 1700 cm<sup>3</sup>, less than 2% of the left lung volume sees  $\geq 50\%$  dose.

### C. Patient surface to radiation source distance changes and effects

Neither the Monte Carlo nor the convolution methods as used herein take into account the changes in dose as the target moves randomly toward or away from the radiation source during each fraction. However, the effects of changes in both the distance from the patient surface to the radiation source (SSD), and the changes in the depth of the target relative to the surface were studied by McCarter and Beckham,<sup>6</sup> wherein they concluded that the variations in position both above and below the mean depth added to give an insignificant net effect, even for very large standard deviations (up to 100 mm). In addition, Bel *et al.*<sup>3</sup> quantified the SSD effect to be less than 1% for a relatively large, one-time 7.5 mm shift along the beam trajectory of one beam in a 3-beam plan.

### D. EEBH versus DIBH

Using end-inspiration breath-holds to compensate for respiratory-derived lung tumor motion results in a less favorable lung mass exposure in the high dose region compared to using an end-expiration breath-holding approach, even after considering the decrease in lung tissue density due to the increased volume of air in the lungs for DIBHs. This is primarily a result of the larger variability in diaphragm position over repeated breath holds at end-inspiration compared to end-expiration, even when lung volume feedback via a spirometer is used in the end-inspiration method and not in the EEBH method. End-expiration breath-holding is therefore recommended over DIBH for fractional radiation therapy of small lung and liver lesions because of improved target position reproducibility, decreased radiation exposure to the surrounding tissue, and because it can be used successfully without the aid of a spirometer or similar device that may diminish patient comfort and compliance.

### E. Mathematical description of target position probability

A goal of subsequent research in this field is to establish the efficacy of using common statistical models, such as a Gaussian distribution, to represent tumor position variability for these lesions. A much larger pool of organ and target repositioning data must be first acquired before any statistical representation can be accepted with confidence. However, the adherence of tumor repositioning to a common statistical model is not strictly required for the application of either the convolution or the Monte Carlo approaches. These methods required only the determination of the 3D target location probability distribution.

### F. Margin size versus target position variability

The current study used the dose field sampled from a treatment plane using clinical margins of  $7 \times 7 \times 10$  mm (AP  $\times$  R  $\times$  SI). These margins are large in comparison to the expected and tested target position variability values, thus the effect of target position variability on the tumor DVH re-

sponse was correspondingly small. Dose broadening studies on dose fields created using smaller treatment margins produce larger changes in the tumor DVH response (data not presented), but the nature of the response remains the same.

### G. Future work

Breath-holding enables us to reduce margin size such that a lethal dose can be administered to the tumor while the volume of healthy tissue receiving toxic dose is kept within clinically acceptable limits. However, radiation toxicity to the surrounding tissue remains a major concern. In our initial patient treatment protocol, a margin size of  $7 \times 7 \times 10$  mm was used for each of five lesions. For a representative 12 mm diameter lesion, 11.3cc of total tissue volume is thereby irradiated with lethal dose, of which only 8% is the tumor. For five such lesions in a patient, a total of 52cc of healthy tissue is destroyed, along with an equally large volume of lung tissue exposed to harmful but nonlethal levels of radiation. In otherwise healthy patients, this loss of lung tissue volume does not pose a serious health risk; however it is conceivable that additional lung lesions may present in these patients over their lifetimes. The cumulative loss of lung volume for a larger number of sites may prove clinically significant. An application of our ability to model the dose erosion effects due to target repositioning error is to improve the methods used for selecting treatment margins. We hope to determine, for each patient, optimal margins that will minimize the volume of surrounding healthy tissue that is irradiated with harmful dose while delivering a lethal dose to each tumor.

### V. CONCLUSION

During fractionated radiotherapy, target position variability over repeated breath-holds will broaden and diminish the amplitude of the dose distribution seen by the target and surrounding tissue, compared with that seen by a fixed target. If the distribution of target positions can be described by a probabilistic model, then this dose-erosion effect can be quantified using image convolution theory and Monte Carlo simulation. Using dose distributions acquired from radiotherapy treatment plans, we have shown that the changes in the dose distribution for target position variability of less than 1 mm are negligible. Using pretreatment MRI acquisitions over repeated breath-holds, we were able to estimate the expected target repositioning error for an individual subject and use this to predict the changes in the dose field that occurred during the subsequent treatment. We were then able to show that the entire tumor was subjected to a cumulative dose in excess of 47 Gy—well above the tumoricidal threshold. This result was supported by the 6- and 12-month clinical follow-up findings wherein all five lesions treated in this patient were eradicated with no evidence of disease recurrence at the treatment sites. This information suggests that curative treatment of lung and liver lesions is possible when simple end-expiration breath holding is used to compensate for respiratory-derived motion. In the future, it is conceivable that all treatment planning of extra-cranial targets will

take into consideration the effects of target repositioning error assessed prior to treatment, further improving the expected clinical outcome for these patients.

## ACKNOWLEDGMENTS

The authors wish to acknowledge the contributions from Emma Gerzhog and Dr. Calvin Maurer, Jr. Financial support of this project was provided through a research agreement with BrainLAB AG (Ammerthalstrasse 8, 85551 Heimstette, Bundesrepublik Deutschland).

<sup>a)</sup>Author to whom correspondence should be addressed. Electronic mail: wodell@rochester.edu

<sup>b)</sup>Also at Department of Biomedical Engineering.

<sup>1</sup>B. K. Lind, "Optimal radiation beam profiles considering uncertainties in beam patient alignment," *Acta Oncol.* **32**, 331–342 (1993).

<sup>2</sup>V. Rudat, "Influence of the positioning error on 3D conformal dose distributions during fractionated radiotherapy," *Radiother. Oncol.* **33**, 56–63 (1994).

<sup>3</sup>A. Bel, "Target margins for random geometrical treatment uncertainties in conformal radiotherapy," *Med. Phys.* **23**, 1537–1545 (1996).

<sup>4</sup>J. H. Killoran, "A numerical simulation of organ motion and daily setup uncertainties: implications for radiation therapy," *Int. J. Radiat. Oncol., Biol., Phys.* **37**, 213–221 (1997).

<sup>5</sup>J. C. Stroom, "Inclusion of geometrical uncertainties in radiotherapy treatment planning by means of coverage probability," *Radiother. Oncol.* **47**, 297–302 (1998).

<sup>6</sup>S. D. McCarter, "Evaluation of the validity of a convolution method for incorporating tumor movement and set-up variations into the radiotherapy treatment planning system," *Ann. Surg.* **231**, 689–700 (2000).

<sup>7</sup>A. Lujan *et al.*, "Quantization of setup uncertainties in 3-D dose calculations," *Med. Phys.* **26**, 2397–2402 (1999).

<sup>8</sup>A. E. Lujan, "A method for incorporating organ motion due to breathing into 3D dose calculations," *Med. Phys.* **26**, 715–720 (1999).

<sup>9</sup>M. A. Hunt, "The effect of setup uncertainties on the treatment of nasopharynx cancer," *Int. J. Radiat. Oncol., Biol., Phys.* **27**, 437–447 (1993).

<sup>10</sup>Cancer Facts and Figures 2002. 2002, American Cancer Society.

<sup>11</sup>S. L. Parker *et al.*, "Cancer statistics, 1997" [published erratum appears in *Ca-Cancer J. Clin.* **47**, 68 (1997)], *Ca-Cancer J. Clin.* **47**, 5–27 (1997).

<sup>12</sup>R. A. Willis, *The Spread of Tumors in the Human Body*, 3rd ed. (Butterworth, London, 1973).

<sup>13</sup>H. A. Gilbert and A. R. Kagan, "Metastases: incidence, detection, and evaluation without histologic confirmation," in *Fundamental Aspects of Metastasis*, edited by L. Weiss (North-Holland, Amsterdam, The Netherlands, 1976), p. 385–405.

<sup>14</sup>R. Stangl *et al.*, "Factors influencing the natural history of colorectal liver metastases," *Lancet* **343**, 1405–1410 (1994).

<sup>15</sup>S. H. Landis *et al.*, "Cancer statistics, 1998," *Ca-Cancer J. Clin.* **48**, 6–29 (1998) [published errata appear in *Ca-Cancer J. Clin.* **48**, 192 (1998) and **48**, 329 (1998)].

<sup>16</sup>F. Bozzetti *et al.*, "Comparing surgical resection of limited hepatic metastases from colorectal cancer to non-operative treatment," *Eur. J. Surg. Oncol.* **19**, 162–167 (1993).

<sup>17</sup>Y. Fong, L. H. Blumgart, and A. M. Cohen, "Surgical treatment of colorectal metastases to the liver," *Ca-Cancer J. Clin.* **45**, 50–62 (1995).

<sup>18</sup>H. C. Andrews and B. R. Hunt, *Digital Image Restoration* (Prentice-Hall, Englewood Cliffs, NJ, 1977), p. 238.

<sup>19</sup>J. Leong, "Implementation of random positioning error in computerized radiation treatment planning systems as a result of fractionation," *Phys. Med. Biol.* **32**, 327–334 (1987).

<sup>20</sup>W. Press *et al.*, *Numerical Recipes in C, The Art of Scientific Computing*, 2nd ed. (Cambridge University Press, Cambridge, England, 1988).

<sup>21</sup>A. Holland, J. Goldfarb, and R. Edelman, "Diaphragmatic and cardiac motion during suspended breathing: preliminary experience and implications for breath-hold MR imaging," *Radiology* **209**, 483–489 (1998).

<sup>22</sup>J. Balter *et al.*, "Improvement of CT-based treatment-planning models of abdominal targets using static exhale imaging," *Int. J. Radiat. Oncol., Biol., Phys.* **41**, 939–943 (1998).

<sup>23</sup>H. Korin *et al.*, "Respiratory kinematics of the upper abdominal organs: a quantitative study," *Magn. Reson. Med.* **23**, 172–178 (1992).

<sup>24</sup>J. Hanley *et al.*, "Deep inspiration breath-hold technique for lung tumors: the potential value of target immobilization and reduced lung density in dose escalation," *Int. J. Radiat. Oncol., Biol., Phys.* **45**, 603–611 (1999).

<sup>25</sup>M. C. Schell *et al.*, "Evaluation of Novalis ExacTrac Patient Positioning System and application to treatment of lung and liver lesions," *Med. Phys.* **28**, 1278 (abstract) (2001).